catalysts

MDPI

Article

Effect of Size and Distribution of Ni Nanoparticles on γ-Al_2O_3 in Oleic Acid Hydrodeoxygenation to Produce *n*-Alkanes

Manuel Sánchez-Cárdenas [1,*], Jorge Medina-Valtierra [2], Sathish-Kumar Kamaraj [1], Rodolfo Rafael Medina Ramírez [1] and Luis Antonio Sánchez-Olmos [1]

[1] Ingeniería en Energía, Universidad Politécnica de Aguascalientes, Calle Paseo San Gerardo 207, Aguascalientes, Ags C.P.20342, Mexico; sathish.bot@gmail.com (S.-K.K.); rodolfo.medina@upa.edu.mx (R.R.M.R.); luis.sanchezo@upa.edu.mx (L.A.S.-O.)

[2] Departamento de Ingeniería Química y Bioquímica, Instituto Tecnológico de Aguascalientes, Av. Adolfo López Mateos #1801 Ote., Aguascalientes, Ags C.P.20256, Mexico; jormeval@yahoo.com

* Correspondence: manuel.sanchez@upa.edu.mx; Tel.: +52-449-256-0292

Academic Editor: Keith Hohn
Received: 4 July 2016; Accepted: 21 September 2016; Published: 19 October 2016

Abstract: To contribute to the search for an oxygen-free biodiesel from vegetable oil, a process based in the oleic acid hydrodeoxygenation over Ni/γ-Al_2O_3 catalysts was performed. In this work different wt % of Ni nanoparticles were prepared by wetness impregnation and tested as catalytic phases. Oleic acid was used as a model molecule for biodiesel production due to its high proportion in vegetable oils used in food and agro-industrial processes. A theoretical model to optimize yield of *n*-C_{17} was developed using size, distribution, and wt % of Ni nanoparticles (NPs) as additional factors besides operational conditions such as temperature and reaction time. These mathematical models related to response surfaces plots predict a higher yield of *n*-C_{17} when physical parameters of Ni NPs are suitable. It can be of particular interest that the model components have a high interaction with operation conditions for the *n*-C_{17} yields, with the size, distribution, and wt % of Ni NPs being the most significant. A combination of these factors statistically pointed out those conditions that create a maximum yield of alkanes; these proved to be affordable for producing biodiesel from this catalytic environmental process.

Keywords: Ni/γ-Al_2O_3 catalysts; oleic acid hydrodeoxygenation; *n*-C_{17} alkane; statistical analysis; response surfaces

1. Introduction

Atmospheric pollution due to fossil fuel consumption is a main factor in global warming. The high rates of non-renewable fuels consumption is leading to a shortage of oil supplies and deepening economic and energetic dependence on oil [1–3].

This condition has fostered research into renewable fuels conducted by academics, governments, and private institutions to develop and adopt new environmentally friendly fuels. Biodiesel produced from used vegetable oil through transesterification reactions is a good option to replace or be added to regular diesel, being an efficient and environmentally friendly alternative [4].

Catalytic hydrotreating of vegetable oils and animal fats is an option to overcome biodiesel disadvantages like oxidative stability and flowing in cold conditions, among others [4]. This process removes oxygen from triglycerides through decarbonylation, decarboxylation, or hydrodeoxygenation (HDO) to produce mainly *n*-alkanes [5–7].

Recent research on HDO shows the catalytic effect of nickel oxalate on alumina (NiO_X/Al_2O_3) for an oleic acid hydrodeoxygenation reaction producing mixtures of *i*-C_{18} and *n*-C_{18} alkanes at 360 °C and 20 bar on a semi-batch reactor [8].

Monnier et al. [9], tested molybdenum, tungsten, and vanadium nitrides onto γ-Al_2O_3 in the HDO of oleic acid and canola oils using a continuous flow microreactor at 380 °C and 7.15 MPa of H_2. By comparing catalysts consisting of metallic nitride supported on γ-Al_2O_3 in canola oil transformation, molybdenum nitride showed a higher conversion rate (obtaining 38 to 48 wt % of biodiesel) than tungsten and vanadium nitrides. Molybdenum nitride mostly promoted oleic acid HDO to *n*-$C_{18}H_{38}$, but a lot less decarbonylation and decarboxylation.

Yang and co-workers synthesized nickel phosphide catalysts onto SBA-15 through programmed temperature reduction and varying the atomic molar ratio of Ni/P to obtain different active phases [5]. Catalysts were tested in the methyl oleate HDO on a continuous flow reactor at 30 bar with the temperature ranging from 250 to 340 °C. They concluded that the activity and product selectivity are significantly affected by the atomic molar ratio of Ni/P.

Hellinger et al. studied the guaiacol HDO using catalysts of Pt supported on SiO_2, Al_2O_3, TiO_2, CeO_2, and ZrO_2 monoclinic zeolites with different ratios of SiO_2/Al_2O_3 (H-MFI-27, H-MFI-55, H-MFI-90, and H-MFI-240) and ZrO_2 tetragonal [10]. These catalysts were prepared through different methods: wetness impregnation, sol-gel precipitation, and flame-spray pyrolysis. Reactions were held on a discontinuous stainless steel reactor at 180 °C, 50 bar of H_2 pressure, and 5 h of reaction time. Product analysis showed that Pt supported on SiO_2 and γ-Al_2O_3 exhibited the highest yield of biodiesel at a temperature up to 200 °C, suggesting that such porous materials are the most used and promising catalytic supports for this process.

Madsen et al. studied the HDO of oleic acid and tripalmitin at more severe conditions on a discontinuous reactor using catalysts with 5 wt % of Ni, Pt and Pd on γ-Al_2O_3 prepared by wetness impregnation [11]. Pd/γ-Al_2O_3 catalysts showed the highest decarboxylation and decarbonylation to hydrogenation.

A recent report from Yang et al. stated that higher yields of ~81% were observed for the decarboxylation of oleic acid to heptadecane over Pt supported on zeolite 5A beads [12]. Ahmadi et al. studied the decarboxylation and selectivity in the conversions of oleic acid to heptadecane with the aid of Pt supported on small-pore zeolites and hydrotalcite. They reported that the increase in the reaction temperature could increase the degree of decarboxylation and improve the selectivity towards heptadecane [13]. Popov and his team tested granulated activated carbon catalysts with formic acid (1% *v*/*v*) as an in situ source of hydrogen; they obtained a heptadecane yield of over 70%, with an 80% selectivity observed between 370 and 380 °C [14]. Srifa et al. studied the deoxygenation of palm oil into green diesel using four supported monometallic catalysts with various metal loadings (2–10 wt % of Co, Ni, Pd, or Pt) on γ-Al_2O_3 prepared by the incipient wetness impregnation method. They observed that the dominant reaction was decarbonylation more than the HDO reaction, when Ni, Pd, and Pt catalysts catalyzed this process. Ni favors the route of decarbonylation by means of C–C bond scission during the transformation of oleic acid to hydrocarbons, although the catalytic activity obeyed the following order: Co > Pd > Pt > Ni [15]. Furthermore, it is known that Ni promotes hydrogen activation, leading to the hydrogenolysis of C−O bonds [16,17].

Many industrial applications of the HDO process generally consider the nickel-based catalysts. Even though noble metal catalysts (Pt, Pd, and Ru) are very active for HDO of unsaturated bounds and aromatic rings, they result in high consumption of hydrogen and relatively low abundance, associated with a high price. In addition, the noble metals tend to get easily tainted by the low amount of sulfur in the oils [18]. Thus, noble metals are unfavorable for industrial-scale processes. Furthermore, Ni-type catalysts are non-pyrophoric, non-magnetic, stay dry when they are stored at ambient conditions, and preserve catalytic activity for longer. Hence, these reasons make it attractive to use nickel-based catalysts to find an appropriate industrial-scale process [19].

Tardity et al. studied the surface properties of Ni catalysts and their correlation with catalyst activity on an ethanol steam reforming reaction [20]. They found that after reducing NiO catalysts with hydrogen flow at 600 °C for 2 h and exposing them to air, a significant amount of metallic Ni is covered with a re-oxidation on the particles' surface. Then they analyzed the effect of air exposure and H_2 reduction at 400 °C on the size of Ni NPs and compared results from XPS, TEM, and XRD techniques. From the XPS study, they found that the size of Ni NPs grew by 3.8% after surface oxidization.

The present study focused on oleic acid hydrodeoxygenation, since this acid is considered as an oxygenated organic model molecule that is present at a high ratio in vegetable oils. We formulated and statistically optimized the oleic acid conversion into *n*-C_{17} and *n*-C_{18} alkanes with the aid of surface response methodology. In addition to physical conditions to optimize the HDO reaction such as temperature and reaction time, we included physical parameters of Ni NPs such as wt %, size, and distribution. Further, interactions of Ni NPs parameters with the other physical parameters with respect to the biodiesel yield were studied. This could be useful when experiments are made with different oxygenated organic compounds that are constituents of vegetable oils, animal fats or biodiesel, and as a base to produce biofuels with high energetic value.

2. Results and Discussions

2.1. Physico-Chemical Characterization of the Catalyst

A summary of chemical composition and textural properties of Ni/γ-Al_2O_3 catalysts is given in Table 1, where wt % corresponds to Ni NPs on γ-Al_2O_3. Due to the fact that the same support was used, the specific surface areas (S_{BET}) and average pore volume (APV) of the Ni/γ-Al_2O_3 catalysts have similar values. A slight reduction in the average pore diameter (APD) was observed when Ni loading was increased, which might be directly related to the partial blockage of support pores [15,21]. The elemental composition of the Ni/γ-Al_2O_3 catalyst was determined using energy dispersive X-ray spectroscopy (EDS) and is shown in the same table. Quantified Ni loadings in catalysts agreed with the theoretical amount of Ni on γ-Al_2O_3 (3, 5, and 7 wt %). A slight variation in the experimental amount for Ni from the expected value was found because EDS is a punctual analysis technique [8].

Table 1. Chemical composition and textural parameters of Ni/γ-Al_2O_3 catalysts.

Sample	Ni, wt %	EDS, wt %			EDS, Atomic %			Textural Properties		
		O	Al	Ni	O	Al	Ni	S_{BET} (m^2/g)	APV (cm^3/g)	APD (nm)
NAL3	3	55.46	41.72	2.82	68.49	30.56	0.95	158.5	0.428	7.22
NAL5	5	50.58	44.26	5.16	64.66	33.55	1.8	147.4	0.405	6.78
NAL7	7	48.11	44.65	7.24	62.84	34.59	2.68	133.8	0.384	6.21

XRD patterns of Ni/γ-Al_2O_3 catalysts (Figure 1) can determine the effect of active phase concentrations on the intensity of the reflections. The diffraction patterns of samples show reflections 2θ at 37.2°, 39.8°, 46.2°, 67.1°, 18°, and 60°; which are characteristic of the crystalline alumina phase [21,22].

XRD diffractograms of catalysts are similar to those of γ-Al_2O_3; this can be attributed to the small quantity of metal introduced. Its presence did not change the crystalline phase of γ-Al_2O_3. The main peaks corresponding to the probable introduction of NiO into the material at 37° and 43° [23] were not recorded in the DRX pattern due to the overlap with the γ-Al_2O_3 intense peaks. Nevertheless, the presence of Ni was detected on the Ni/γ-Al_2O_3 catalysts since the weak peak at ~77° corresponds to the crystallites of Ni [24], which is almost undetectable in the NAL-3 sample.

Figure 2a shows XPS spectra of Ni/γ-Al_2O_3 catalysts with different weight percentages of Ni (3, 5, and 7). The O1s spectrum characteristic of oxygen is clearly observed at a binding energy at 530 eV. Al2p can be observed with a typical binding energy of 74 eV [25]; thus, it was determined that the Al atoms are in the oxide form, and can act as catalyst supports [26]. Figure 2b shows the peaks in the range between 850 and 900 eV. The most intense peak was detected at 856.08 eV, and corresponds

to the Ni 2p3/2 state. Two satellite peaks of Ni 2p3/2 were observed at 861.86 and 880.14 eV that are characteristic for Ni^{2+} species [27–30]. On the other hand, the basic spectrum shows the Ni 2p1/2 state at 873.94 eV attributed to Ni^{3+} species [31]. This could be explained by the exposure of catalysts to the ambient promoting oxidation on the catalyst surface. However, during the HDO reaction, an in situ reduction of some oxide species on the surface of Ni catalyst is performed, resulting in only Ni/Al_2O_3 [20]. The experimental composition calculated from XPS analysis was 2.6, 4.4, and 6.2 wt % compared to the theoretical composition of 3, 5, and 7 wt % of Ni, respectively. The weight percentage obtained through this analysis confirms that the method of preparation of the catalysts was adequate and in accordance with EDS.

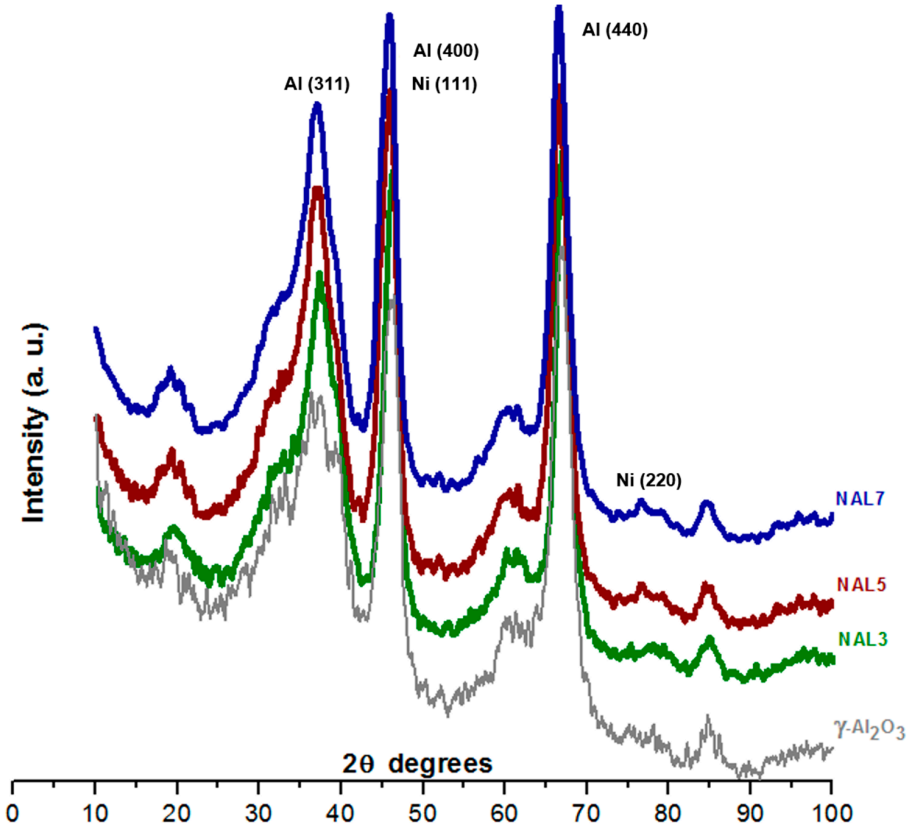

Figure 1. Patterns of X-ray diffraction of Ni/γ-Al_2O_3 catalysts and γ-Al_2O_3 support.

The influence of different Ni loadings in the nanoparticle morphology deposited on γ-Al_2O_3 was studied by high-resolution transmission microscopy (HR-TEM). According to Figure 3, the particle size of the Ni phase slightly increases, while the Ni loading is increased over the support material. Histograms of Ni nanoparticles (Figure 4) show an increase in the average size with respect to the weight percentage of metal loaded; over 1.8–4.6 nm, 3.2–5.3 nm, and 4.6–6.5 nm for NAL3, NAL5, and NAL7 samples, respectively. The wet impregnation technique followed by oxidation and reduction processes were adequate to deposit and disperse Ni NPs, where the role of HNO_3 enhanced the properties of the crystalline structure of γ-Al_2O_3 (mainly planes 100, 110, and 111), as reported by Digne et al. [32]. The properties of γ-Al_2O_3 are determined by various surface conditions, mainly the increase in surface hydroxyl groups, which can produce Ni nanoparticles of smaller sizes. Figure 3d shows the STEM image of 5 wt % of Ni NPs supported on γ-Al_2O_3, where lattice fringes of Ni atoms and a slightly oval shape of nanoparticles can be observed.

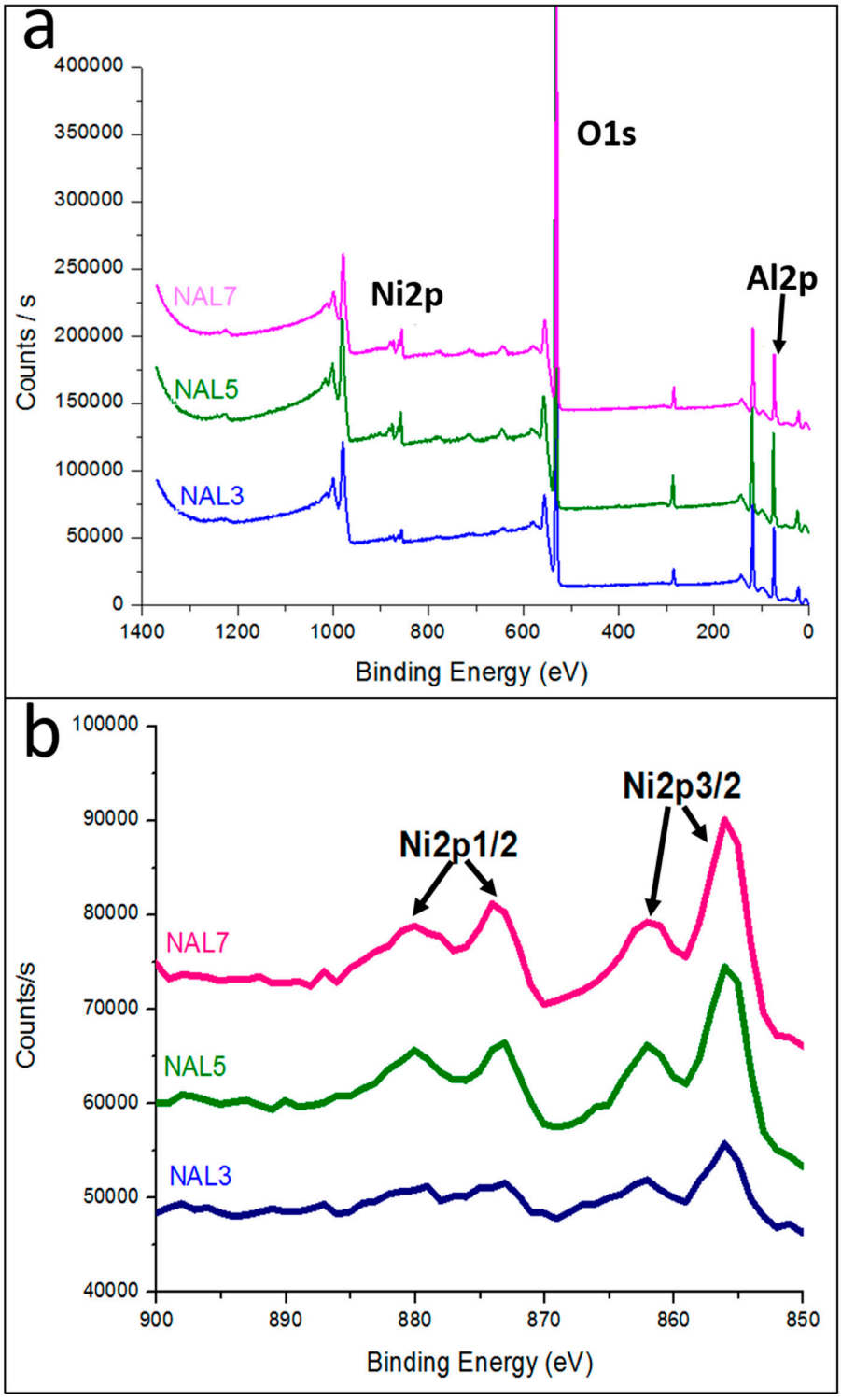

Figure 2. (**a**) XPS spectra general of Ni/γ-Al_2O_3 catalysts; (**b**) identification of the Ni states in these catalysts.

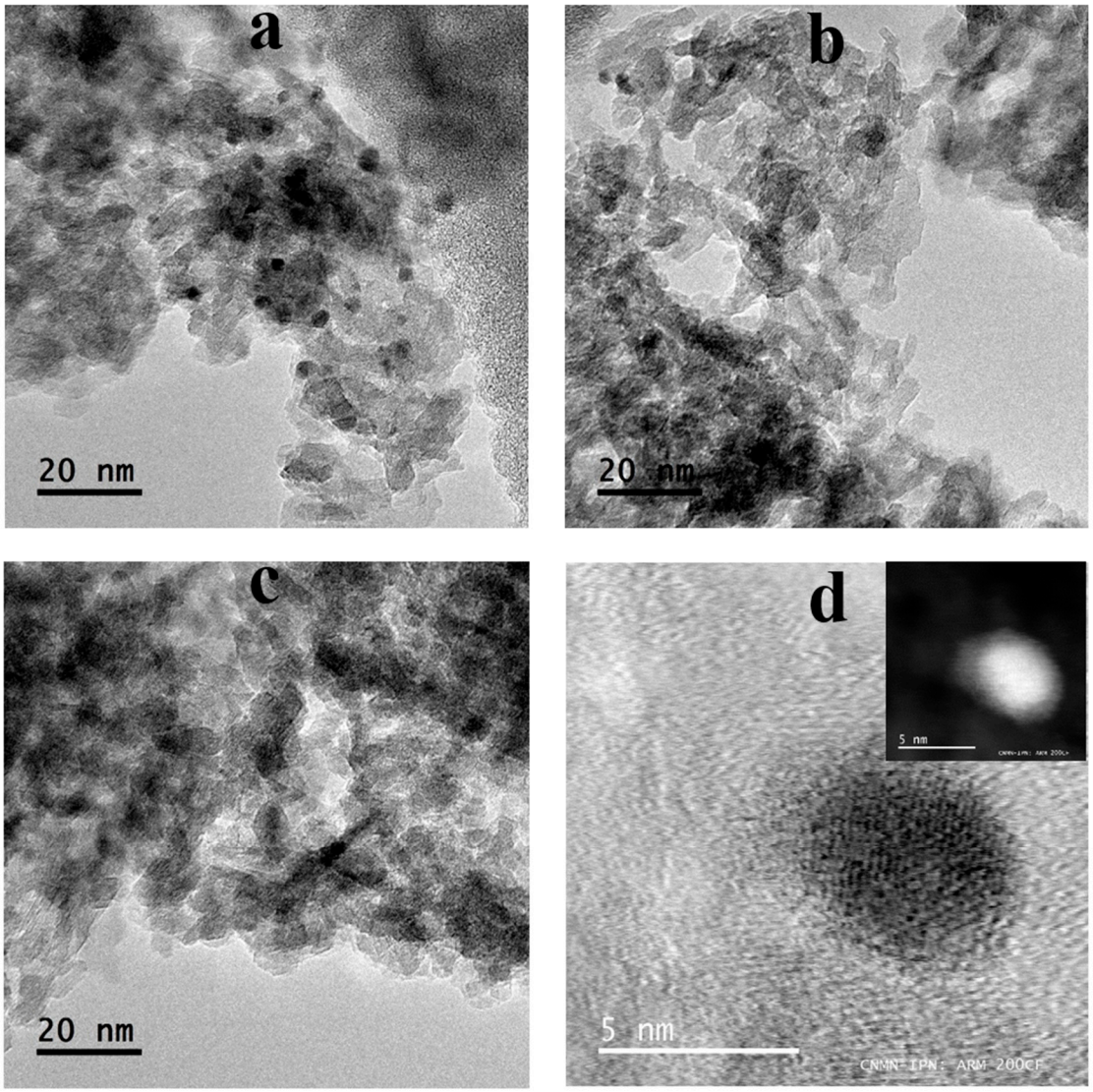

Figure 3. TEM micrographs of Ni/γ-Al_2O_3 catalysts: (**a**) NAL3; (**b**) NAL5; (**c**) NAL7; and (**d**) lattice fringes of Ni NPs on the NAL5 catalyst.

A multivariate analysis considering the size and amount of Ni nanoparticles deposited was performed using the Statgraphics software. Table 2 shows a statistical analysis of Ni nanoparticles size, including central tendency and dispersion measurements. For all Ni/γ-Al_2O_3 catalysts (3, 5, and 7 wt % of metal) it can be observed that the standardized bias and standardized kurtosis indicate that the size of the Ni nanoparticles deposited is normally distributed, because these values are within the statistical range of -2 to +2. This study also found that the average nanoparticle size variation coefficient increases as the weight percentage of Ni increases. The coefficient of variation is of particular interest since it is a measurement of dispersion that is defined as the ratio between the average size and the variable range. It was noted that a higher coefficient of variation implies a greater dispersion of Ni nanoparticle size (Table 2).

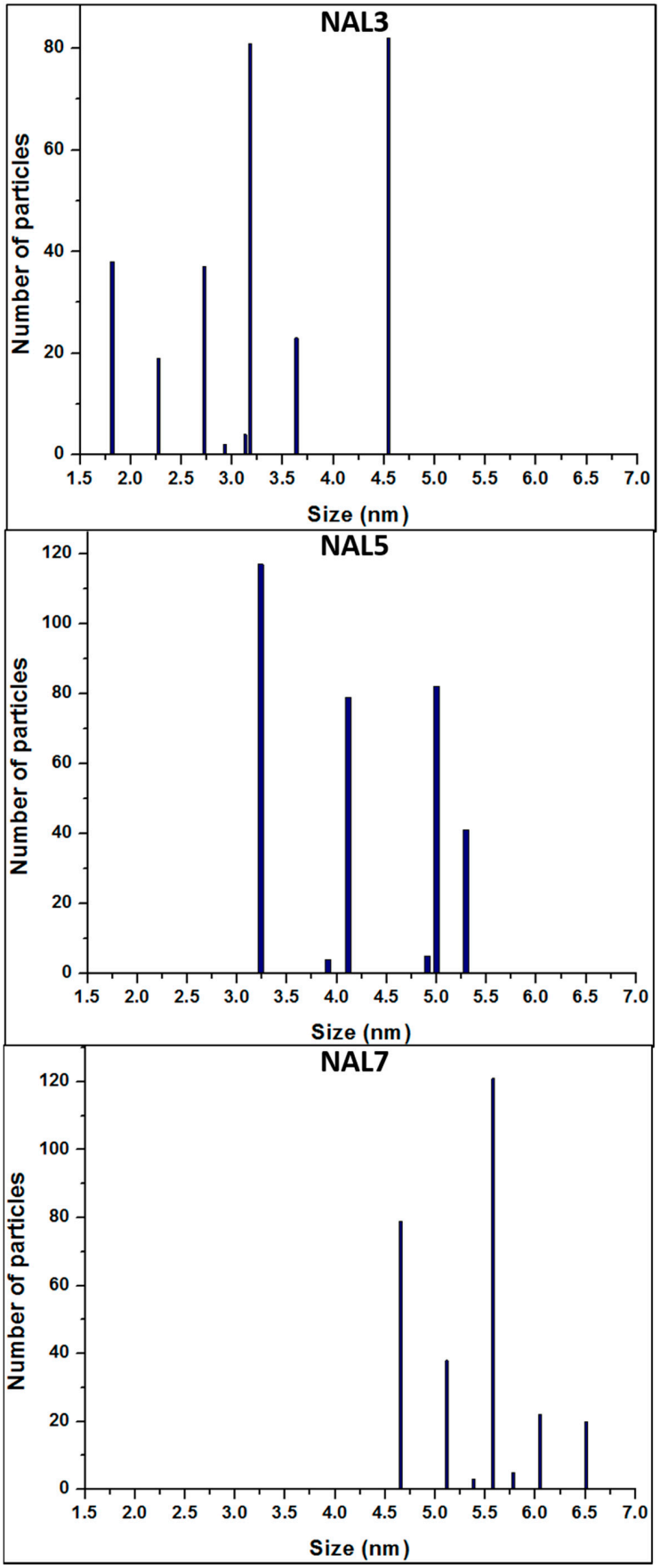

Figure 4. Histograms of particle size in Ni/γ-Al_2O_3 catalysts: NAL3, NAL5, and NAL7.

Table 2. Statistical analysis for Ni nanoparticles size deposited on γ-Al_2O_3.

Statistical	Ni Loading, wt %		
	3	5	7
Average size of Ni NPs (nm)	3.03	4.41	5.58
Coefficient of variation of Ni NP size distribution (%)	31.40	32.51	34.29
Standardized bias	0.4629	−0.5163	0.2614
Standardized kurtosis	−0.15	−0.6940	−0.5432

2.2. Conversion of Oleic Acid by Hydrodeoxygenation

Yields of *n*-C_{17} and *n*-C_{18} in the oleic acid HDO were compared for all Ni /γ-Al_2O_3 catalysts. It can be concluded that the density and size of Ni nanoparticles accelerate HDO reaction into the homemade reactor. As mentioned before, the reaction temperature varied from 320 to 340 °C; H_2 pressure remained in 23 bar; stirring was kept steady at 120 rpm; and the reaction time was 4–5 h, with acid oleic conversion and product yield calculated by GC analysis.

NAL7 at 320 °C gave a conversion of 75.4% after 4 h reaction time; NAL5 and NAL3, after the same reaction time, showed conversions of 69.7% and 57.9%, respectively. Hence, a higher load of Ni on alumina gives higher conversion, according with reports in the current literature of catalytic activity on Pt /γ-Al_2O_3, Pd/γ-Al_2O_3 y Ni/γ-Al_2O_3 [11]. After 5 h of reaction time at 340 °C, NAL7 again gave a higher oleic acid conversion (84.8%) in comparison with NAL5 and NAL3, which showed conversion rates of 79.4% and 70.1%, respectively. It can preliminarily be concluded that operation conditions, Ni NPs as catalytic phase, and a reactor with axial/radial stirring produce adequate conversion at short reaction times in similar experiments, as previously reported by Madsen et al. [11].

Yields of *n*-C_{17} and *n*-C_{18} from oleic acid decarbonylation and decarboxylation at 320/340 °C and 4–5 h reaction times are analyzed in Figure 5. In all experiments the NAL7 catalyst showed a better yield of *n*-C_{17} (i.e., 68.94 mol % at 340 °C after 5 h). All catalysts showed higher yields of alkanes *n*-C_{17} and *n*-C_{18} after 5 h of reaction time. On the other hand, a higher temperature produces decarbonylation and decarboxylation reactions, mainly producing *n*-C_{17} [33]. After 5 h, the *n*-C_{17} yield was higher at 340 °C, giving similar results using a catalytic material with 7 wt % of Ni, as reported by Kaewmeesri et al. [34]. However, changes in the product yields are more notable in the NAL5 catalyst when experimental data are compared after 4 h of reaction time with those at 5 h.

Analyzing the experimental results, it may be observed that after 4 and 5 h of reaction time, the *n*-C_{17} yield is just a little higher for NAL7. However, 5 wt % of Ni loading seems to be a better catalyst from a cost-benefit point of view to assure high oleic acid conversion rates and a good *n*-C_{17} selectivity based on the active phase percentage used on industry [11]. Our results are consistent with those of Kubicka et al., who reported higher conversion on hydrotreatment of vegetable oils when higher proportions of Ni/(Ni + Mo) to Al_2O_3 were used [35]. Strobel and co-workers [36] found that an increase in the quantity of Pt nanoparticles causes an increase in the catalyst intrinsic activity and yield during hydrogenation reactions; this behavior could also be applied to Ni and Pd, which along with Pt are metals capable of accelerating and conducting HDO reactions but with different efficiency. Our results infer that the increasing weight percentage of Ni NPS could produce higher *n*-C_{17} yield after a short reaction time.

A small portion of the spent catalyst was recovered by filtering and drying treatments. The appearance of the dry catalyst did not change significantly after the reaction and retains a pale blue color, the same as the original catalyst. Hence, these catalysts may have a high degree of resistance to deactivation in HDO reactions under the conditions used in this work.

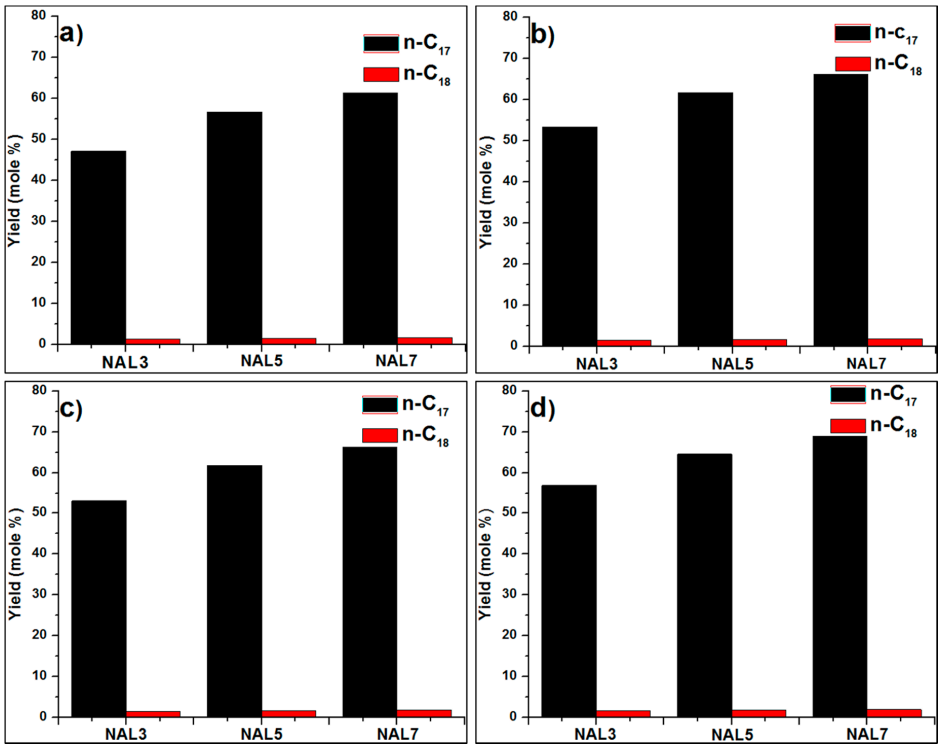

Figure 5. Yields of n-C_{17} and n-C_{18} from oleic acid hydrodeoxygenation on Ni/γ-Al_2O_3 catalysts: (**a**) 4 h, 320 °C; (**b**) 5 h, 320 °C; (**c**) 4 h, 340 °C; and (**d**) 5 h, 340 °C.

Table 3 shows a comparison of the n-C_{17} obtained during the hydrodeoxygenation of oleic acid with different catalysts. It clearly shows an increase in the yield of n-C_{17} with the catalyst NAL5, when it was compared to the yield obtained with a similar catalyst [15]. Additionally, the NAL7 catalyst showed a similar yield with that reported containing 10 wt % of Ni [34]. These results are promising and confirm that the reaction conditions and the type of agitation of the reactor used in our reaction potentiate the catalytic properties of Ni/γ-Al_2O_3. n-C_{17} yields for NAL5 and NAL7 catalysts are slightly higher than yields shown by Pt (5 wt %), Co (5 wt %), and Ni (5 wt %) supported on γ-Al_2O_3. However, Pt/zeolite 5A beads (1 wt %) and Pd/γ-Al_2O_3 (5 wt %) exhibited higher yields of 81.5% and 72%. Nevertheless, the higher cost of noble metals hinders their use as catalytic phase for industrial-scale processes. A preliminary conclusion can be: NAL7 yield is close to that shown by the granulated activated carbon catalyst [14], and shows a higher catalyst performance compared to 5 wt % Pt supported on small-pore zeolites [13].

Table 3. n-C_{17} yields with Ni/γ-Al_2O_3 catalysts and other catalysts in the oleic acid hydrodeoxygenation.

Catalyst	Catalyst Composition	Reaction Conditions	Main Reaction Product	Yield	Reference
NAL3	3 wt % Ni	0.9 g of catalyst, P = 23 bar, T = 340 °C, t = 5 h.	n-C_{17}	56.95%	This work
NAL5	5 wt % Ni		n-C_{17}	64.55%	This work
NAL7	7 wt % Ni		n-C_{17}	68.94%	This work
Pt/zeolite 5A beads	1 wt % Pt	metal/oleic acid (wt %) = 1:100, P = 20 bar, T = 320 °C, t = 2 h.	n-C_{17}	81.5%	12
Granulated activated carbon	1% v/v formic acid	18.2 g of catalyst, P = 24.1 MPa, T = 350 to 400 °C, WHSV = 4 h^{-1}.	n-C_{17}	70%	14
5Co/γ-Al_2O_3	5 wt % Co	LHSV of 2 h^{-1}, H_2/fatty acid, ratio of 1000 N(cm^3/cm^3) P = 5 MPa, T = 330 °C.	n-C_{17}	47%	15
5Co/γ-Al_2O_3	5 wt % Co		n-C_{18}	53%	15
5Ni/γ-Al_2O_3	5 wt % Ni		n-C_{17}	25.5%	15
5Pd/γ-Al_2O_3	5 wt % Pd		n-C_{17}	72%	15
5Pt/γ-Al_2O_3	5 wt % Pt		n-C_{17}	51.1%	15
10Ni/γ-Al_2O_3	10 wt % Ni	LHSV of 2.0 h^{-1}, H_2/oleic acid, ratio of 1000 $cm^3 \cdot cm^{-3}$, P = 50 bar, T = 330 °C, T = 330 °C	n-C_{17}	81.3%	34
Pt-SAPO-34	5 wt % Pt	2 g of catalyst, P = 20 bar, T = 355 °C, t = 2 h.	n-C_{17}	66.9%	13

As an additional approach to analyze NPs' characteristics and their effect on n-C_{17} production, a regression model was developed to measure the correlations among physical variables and process conditions. Three polynomial models were developed to predict the yield of n-C_{17} based on temperature (T), reaction time (t), and any of the three physical variables that complete this statistical study, i.e., Ni wt % (W), average particle size (S), and dispersion of Ni nanoparticles (V), where S and V were calculated statistically from TEM images of the catalyst (Figure 3). The comparison of these important catalytic parameters (W, S, and V) related to catalytic performance is a major contribution of this paper. Statistical models are based on the polynomial regression methodology and consequently are used to obtain response surface plots. In this work three polynomial models were obtained with different independent variables including the three variables that represent the Ni NP parameters: Model 1A with T, t, and W as variables; Model 1B with T, t, and S as variables; and Model 1C with T, t, and V as variables. Statistical coefficients, Fisher ratio (***F***), and ***p***-value for molar yield of n-C_{17} are shown in Table 4. Corresponding variables will be significant if the p-value becomes smaller and the value of ***F***-ratio is higher than the statistical value of ***F*** (1, 5, 0.05). Table 4 shows that the values of statistical coefficients ***F***-ratio and ***p***-value are equal for the polynomial models, which confirms that the statistical analysis describes and relates an important application of the W, S, and V variables (Table 2). This statistical study defines a general polynomial regression model to predict the yield of n-C_{17} (see Equation (A.1)). Values of ***F***-ratio and ***p***-value as well as predicted equations are shown in the same table.

Table 4. Statistical coefficients for n-C_{17} yield (mol %) and their statistical significances.

Model 1A Where *X* is the Ni wt % (*W*)				
Var.	**Coef.**	**B**	***F*-Ratio**	***p*-Value**
	β_0	68.940		
W	β_1	5.9550	420.63	0.0000
T	β_2	1.4500	24.940	0.0041
T	β_3	1.7625	36.850	0.0018
W^2	β_{11}	−6.32125	218.75	0.0000
WT	β_{12}	−0.8625	4.4100	0.0897
Wt	β_{13}	−0.3575	0.7600	0.4238
T^2	β_{22}	−1.92125	20.210	0.0064
Tt	β_{23}	−0.5675	1.9100	0.2255
t^2	β_{33}	−1.33125	9.7000	0.0264
$YC_{17} = 68.94 + 5.955\ W + 1.45\ T + 1.7625\ t - 6.32125\ W^2 - 0.8625\ WT - 0.3575\ Wt - 1.92125\ T^2 - 0.5675\ Tt - 1.33125\ t^2$				
Model 1B, where *X* is the average size of Ni nanoparticles (*S*)				
Var.	**Coef.**	**β**	***F*-Ratio**	***p*-Value**
	β_0	68.940		
S	β_1	5.9550	420.63	0.0000
T	β_2	1.4500	24.940	0.0041
T	β_3	1.7625	36.850	0.0018
S^2	β_{11}	−6.32125	218.75	0.0000
ST	β_{12}	−0.8625	4.4100	0.0897
St	β_{13}	−0.3575	0.7600	0.4238
T^2	β_{22}	−1.92125	20.210	0.0064
Tt	β_{23}	−0.5675	1.9100	0.2255
t^2	β_{33}	−1.33125	9.7000	0.0264
$YC_{17} = 68.94 + 5.955\ S + 1.45\ T + 1.7625\ t - 6.32125\ S^2 - 0.8625\ ST - 0.3575\ St - 1.92125\ T^2 - 0.5675\ Tt - 1.33125\ t^2$				
Model 1C, where *X* is the coefficient of variation of Ni NP size distribution nanoparticles (*V*)				
Var.	**Coef.**	**B**	***F*-ratio**	***p*-value**
	β_0	68.940		
V	β_1	5.9550	420.63	0.0000
T	β_2	1.4500	24.940	0.0041
T	β_3	1.7625	36.850	0.0018
V^2	β_{11}	−6.32125	218.75	0.0000
VT	β_{12}	−0.8625	4.4100	0.0897
Vt	β_{13}	−0.3575	0.7600	0.4238
T^2	β_{22}	−1.92125	20.210	0.0064
Tt	β_{23}	−0.5675	1.9100	0.2255
t^2	β_{33}	−1.33125	9.7000	0.0264
$YC_{17} = 68.94 + 5.955\ V + 1.45\ T + 1.7625\ t - 6.32125\ V^2 - 0.8625\ VT - 0.3575\ Vt - 1.92125\ T^2 - 0.5675\ Tt - 1.33125\ t^2$				

To get a more suitable regression model that predicts yields of n-C_{17}, a Box–Behnken method has been used wherein independent variables are coded and replaced in Model 1. This encoding process presupposes that interception coefficients (βi), determination coefficients ($\mathbf{R}^2$), ***F***-ratio values, and ***p***-values for the three models are equal. To evaluate the goodness of the model fit, an Anova test was run, with the results of the quadratic polynomial model showing that the model adequately described the response surface within the selected range, according to the determination coefficient value of 99.31%.

We must highlight the fact that Ni nanoparticle parameters such as *W*, *S*, and *V* have a high interaction impact with the rest of the other parameters on n-C_{17} yield due to the ***p***-value being lower than 0.05. ***X*** is the variable representing the *W*, *S*, and *V*, as established above; thus ***X*** and $\boldsymbol{X^2}$ are the factors representing the significant impact on the n-C_{17} yield. It is noted that while *T*, *t*, and T^2 are significant, the interaction between parameters *W*-*T*, *W*-*t*, *T*-*t*, and quadratic term t^2 are significant but less important. These results were verified by comparing the values of ***F***-ratio against the value of ***F*** (1, 5, 0.05) = 6.608. Table 5 shows the combination of factor levels, with a maximum yield of n-C_{17} of 70.89% in the specified region. The 3D response surface for the yield of n-C_{17} is shown in Figure 6 for the *T*, *W*, *S*, and *V* variables (Figure 6a), and for the *t*, *W*, *S*, and *V* variables (Figure 6b), where optimization zones are visualized.

Table 5. Combination of factor levels that maximize the yield of n-C_{17} and n-C_{18}.

Factor	Optimum	
	For n-C_{17}	For n-C_{18}
T (°C)	331.95	335.7
t (h)	4.78	4.76
*W*t (%)	5.8834	6.06
S (nm)	4.8681	4.98
V (%)	33.483	33.61

Table 6 shows the calculated coefficient, Fisher-***F***, and ***p***-value for the yield of n-C_{18} (mol%). The criteria for determining the statistical significance are the same as those used for n-C_{17} yield. In all polynomial models it was observed that values of the determination coefficients ***F***-ratio and ***p***-value are equal. This statistical analysis defines the same general polynomial regression model (Equation (1)) used to predict yields of n-C_{18}.

Likewise, for predicting n-C_{17} yield, predictions for n-C_{18} yields from this polynomial model need to use the coded levels of independent variables in Model 2. This encoding process also presupposes that the interception coefficients (βi), determination coefficients ($\boldsymbol{R^2}$), ***F***-ratio values, and ***p***-values for these three models are equal. From the Anova results of the quadratic polynomial model, we found that the model adequately described the response surface in the chosen range, according to the determination coefficient value of 99.14%.

Table 6 shows all ***F***-ratio and ***p***-values for each interaction parameter. Here, ***α*** represents Ni nanoparticle parameters such as W, S ,or V. The values ***α*** and $\boldsymbol{\alpha^2}$ had the greatest effect, while the effects observed for T-t and T^2-t^2 were less significant. These results are verified by comparing the ***F***-ratio against the statistical value of ***F*** (1, 5, 0.05) = 6.608. Table 5 shows the combination of factor levels, with the maximum yield of n-C_{18} being 2.002% in the indicated region. Figure 7 shows the 3D response surface on yields of n-C_{18}, for the T, W, S, and V variables (Figure 7a), and for the t, W, S, and V variables (Figure 7b), where optimization zones also are visualized.

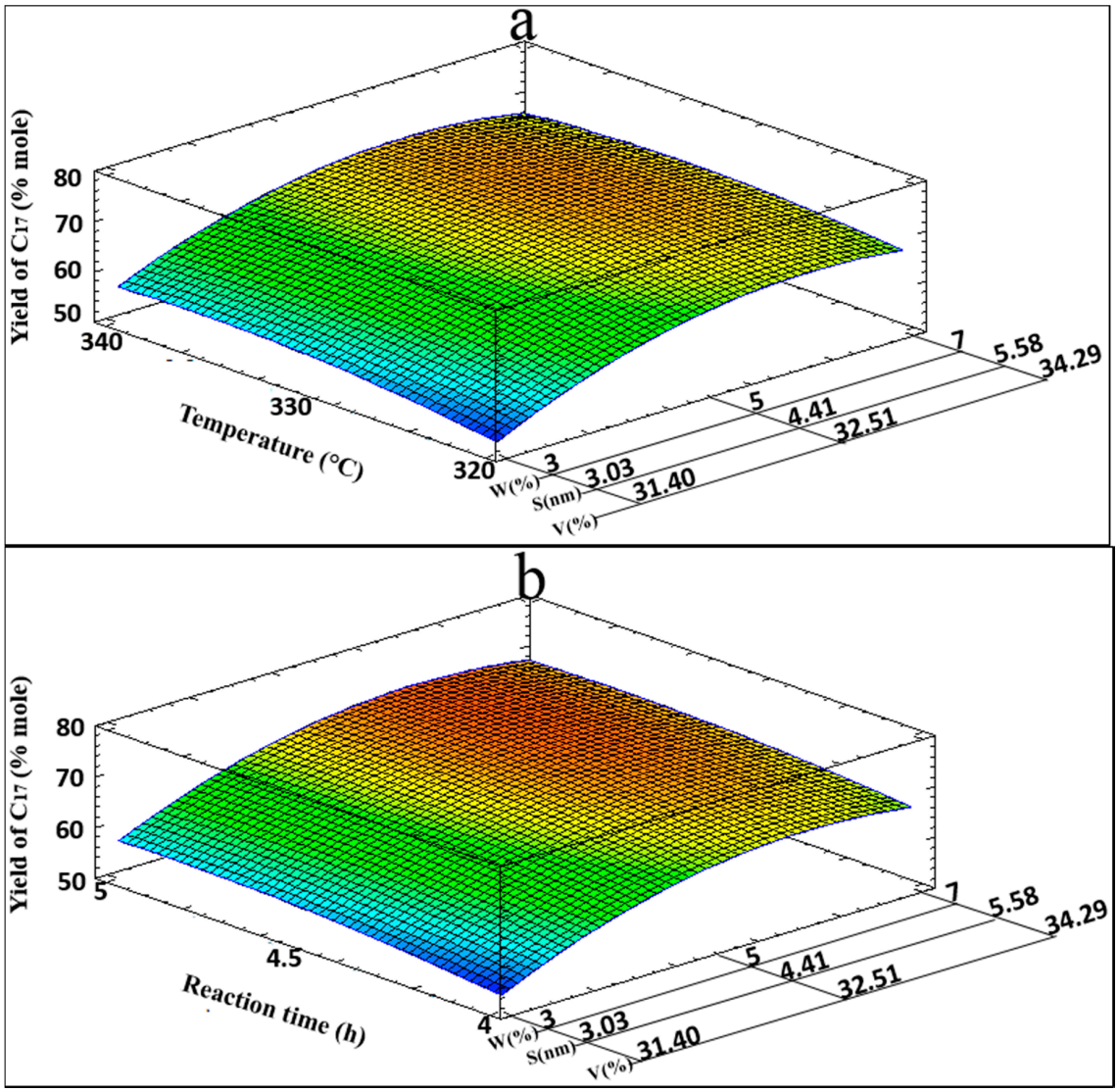

Figure 6. 3D response surface for *n*-C_{17} yield combining: (**a**) *T*, *W*, *S*, and V; (**b**) *t*, *W*, *S*, and *V*.

Table 6. Statistical coefficients for *n*-C_{18} yield (mol %) and their statistical significance.

Model 2				
Var.	**Coef.**	***B***	***F*-Ratio**	***p*-Value**
	β_0	1.92667		
A	β_1	0.17875	371.35	0.0000
T	β_2	0.05125	30.530	0.0027
T	β_3	0.05250	32.030	0.0024
α^2	β_{11}	−0.15958	136.61	0.0001
αT	β_{12}	−0.00750	0.3300	0.5922
At	β_{13}	−0.01000	0.5800	0.4803
T^2	β_{22}	−0.03458	6.4200	0.0523
Tt	β_{23}	−0.01500	1.3100	0.3046
t^2	β_{33}	−0.03708	7.3800	0.0420

$YC_{18} = 1.92667 + 0.17875\ \alpha + 0.05125\ T + 0.0525\ t - 0.159583\ \alpha^2 - 0.0075\ \alpha T - 0.01\ \alpha t - 0.0345833\ T^2 - 0.015\ Tt - 0.0370833\ t^2$

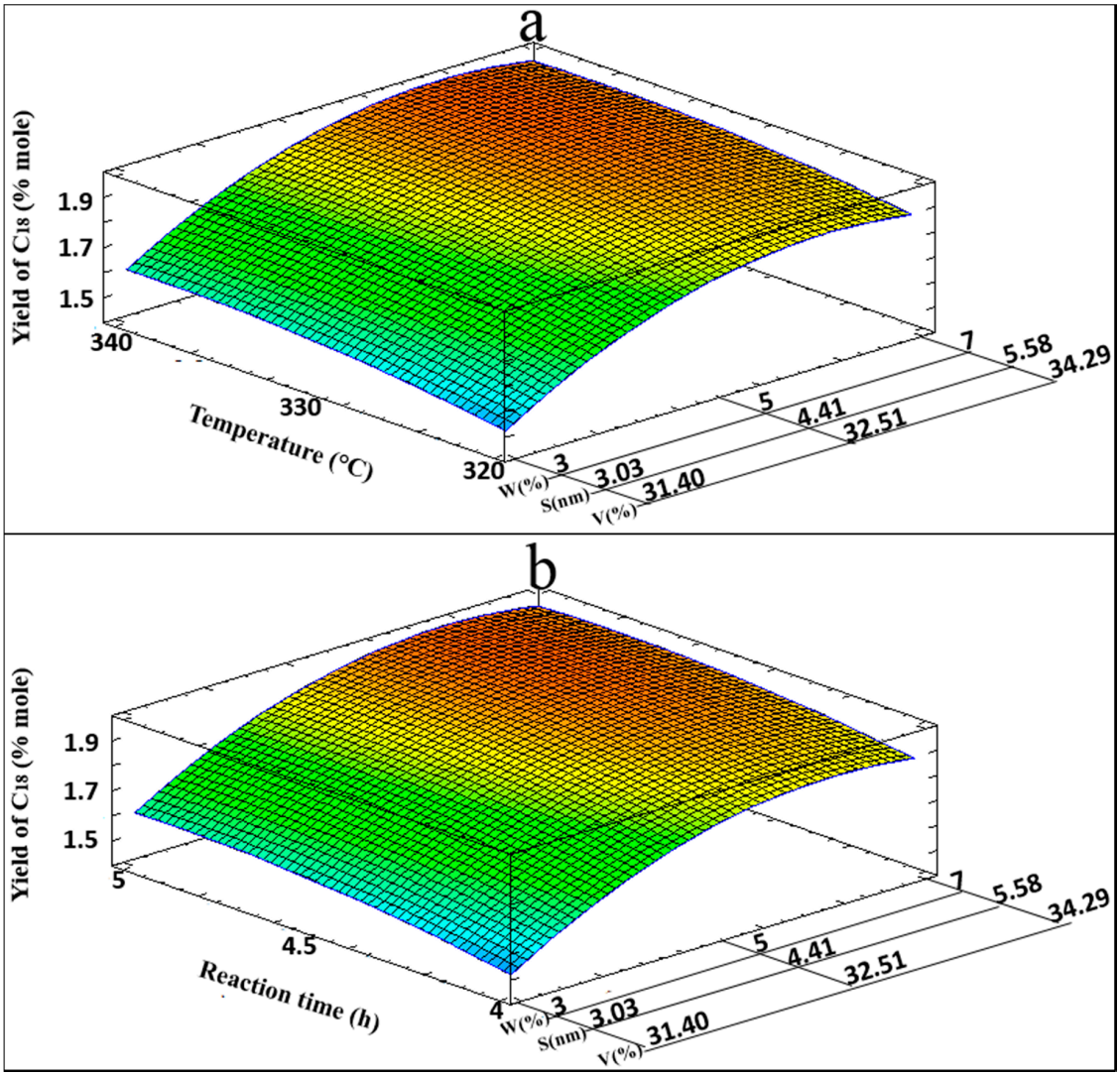

Figure 7. 3D response surface for *n*-C_{18} yield combining: (**a**) T, W, S, and V; (**b**) t, W, S, and V.

From the Anova test applied to *n*-C_{17} and *n*-C_{18} yields, the ***F*** value was used to confirm the validity of the proposed models. In both cases values were higher than ***F*** (9, 5, 0.05) of 4.772, with ***F*** values of 80.29 for *n*-C_{17} and 64.26 for *n*-C_{18}, and $\mathbf{R^2}$ values of 0.9931 and 0.9914, respectively. With a high statistical confidence level, the regression models can predict the maximum yields of *n*-C_{17} and *n*-C_{18}. Every experiment was performed by running two replicates and taking the average of both results to develop theoretical models for yields of *n*-C_{17} and *n*-C_{18}. The standard deviation of the experiments was computed to estimate the reproducibility of the catalytic process. Values for the standard deviation were 0.215 and 0.026, respectively. Hence, it may be concluded that the results reproducibility in this catalytic process is good enough.

3. Materials and Methods

3.1. Catalyst Preparation

Catalytic materials with 3, 5, and 7 wt % of Ni NPs on γ-Al_2O_3 (NAL3, NAL5, and NAL7) were prepared by incipient wetness impregnation method using nickel (II) acetate tetrahydrate, $Ni(OCOCH_3)_2{\cdot}4H_2O$ (Sigma Aldrich, St. Louis, MO, USA, 99.998%) as the metal precursor, which was physically mixed with the required amount of boehmite [AlO(OH)] and ground until a fine blend was

obtained. This wt % range for Ni was determined in recent studies that show promising results for oleic acid hydrodeoxygenation using catalysts containing 5 wt % of Ni [11], which favored the decision to apply a specific range with values around 5 wt % (3, 5, and 7 wt %) in this study. In industrial practice catalysts with 27 wt % of Ni have been used [19]. The resulting blend was made wet by dropping in a small amount of a diluted solution of HNO_3 (J.T. Baker, Xalostoc, Edo. de Méx, México, 67–70 vol %). The active phase was well dispersed into the boehmite by regulating the acid–base balance on the support surface to get a homogeneous paste. To obtain small fibers with the same length, an extrusion process was performed, and then solids were dried at room temperature for 48 h and calcined at 510 °C in oxygen for 4 h to obtain nickel oxide/γ-Al_2O_3 materials. To conclude this procedure, the Ni catalysts were chemically reduced with H_2 flow at 400 °C for 3 h, to obtain a Ni/γ-Al_2O_3 catalyst.

3.2. Catalyst Characterization

A Quadrasorb SI analyzer (Quantachrome Instruments, Dr, Boynton Beach, FL, USA) was used to perform the nitrogen sorption method and, thus, the surface area and pore size distribution of Ni/γ-Al_2O_3 catalysts were determined. Each sample was outgassed at 130 °C overnight before nitrogen sorption at 77.5 K. To obtain the apparent BET surface area (S_{BET}), the BET equation was applied to N_2 adsorption isotherms. The total pore volume was obtained from the amount of N_2 adsorbed at $P/Po = 0.95$ ($V_{0.95}$). The quenched solid density functional theory (QSDFT) was applied to the N_2 adsorption isotherms in order to determine pore size distribution (PSD), average pore volume (APV), and average pore diameter (APD).

X-ray diffractograms were obtained from samples with a Bruker D8 Advance diffractometer (Bruker , Madison, WI, USA)using CuKα radiation (λ = 0.154 nm) and scanned in a 2θ interval of 10°–100° with a rate of 0.02°/s, voltage of 40 kV, and current of 40 mA.

An X-ray photoelectron spectroscopy analysis (XPS) was achieved with a Thermo Scientific (Waltham, MA, USA) model K-Alpha using monochromatized AlKα radiation (1487 eV). XPS spectra were obtained in a high vacuum (10^{-9} mbar) with a spot size of 400 µm over the sample. Narrow scans were recorded at a pass energy of 60 eV and the binding energy values were charge-corrected to the O1s signal (531.0 eV) as an internal standard. From the average of three narrow scans taken from different surface zones, a qualitative analysis was achieved. Assuming that the XPS peaks have a Gaussian–Lorentzian line shape, the Shirley background subtraction method was applied to the proper subtraction of the baseline and the resulting outcomes were divided into individual components.

Samples were analyzed through transmittance electronic microscopy (TEM) using JEOL (Akishima, Tokyo, Japan) JEM-ARM200F equipment with a cold field emission gun operating at 200 kV. Powdered samples were directly dry-sprayed onto a commercially amorphous holey film carbon-coated copper grid. Additionally, an elemental analysis was obtained by energy dispersive X-ray spectroscopy (EDS).

3.3. Oleic Acid Hydrodeoxygenation

HDO experiments were performed using a 200 mL stainless steel reactor that stirs the reaction by the novel means of four paddles that rotate in a vertical axis fixed to the bottom of the reactor; thus, a radial and axial stirring rate of 120 rpm was achieved. In each experiment a Ni/γ-Al_2O_3 catalyst was put into the reactor, and then it was closed and purged with N_2 flow for 2 min to remove the air. H_2 was injected into the reactor until a pressure of 16 bar was reached, then it was heated at 300 °C for 0.5 h to achieve a complete chemical reduction of resulting Ni oxides from the contact of the catalyst with air [11]. Once the reactor was cooled, a mixture consisting of 0.016 mol of oleic acid, 0.2 mol of tetradecane as a solvent (typical amounts for 0.9 g of Ni/γ-Al_2O_3) was placed into the reactor. The same amount of catalyst, but with different Ni loadings, was used in all experiments to evaluate the effect of the amount of active phase for the product yield and selectivity in the oleic acid HDO reaction.

After the reactor was purged with N_2 for 2 min to remove the air, it was again pressurized with H_2 at 16 bar, and the chemical mixture was heated to 320–340 °C to reach a final pressure of 23 bar. The reaction was maintained for 4–5 h at 120 rpm, considering that an increase in the reaction time favors the main product yield [37].

3.4. Analysis of Liquid Products

Gas chromatography analysis was done with equipment that performed the AC 8634 application. This system was developed for samples within 3 and 4 ASTM D86 groups. The application was performed on an Agilent Technologies (Santa Clara, CA, USA) 7890 gas chromatograph, equipped with an AC temperature programmable inlet (TPI) and flame ionization detector (FID). The AC 8634 application uses a fast SIMDIS method to report volume % data according to the D86 testing and true boiling point distribution of alkanes to the carbon length of C_5–C_{44} (high distillation temperature of 545 °C). In this case, carbon disulfide was used as the calibration standard. The AC 8634 software uses a correlation technique to convert SIMDIS data to D86 data for directly measuring the alkanes content.

3.5. Development of Regression Models and Statistical Analysis

To determine the effect of operational factors on the chemical process described above and their interactions, a design of experiments (DOE) was conducted to measure the degree of correlation among the multiple variable involved in the oleic acid HDO and its conversion to *n*-C_{17} and *n*-C_{18} alkanes. The experimental factors chosen to execute the DOE were temperature (T), reaction time (t), Ni wt % (W), average size of Ni nanoparticles (S), and coefficient of variation of size distribution of Ni nanoparticles (V). Table 7 shows the range of values and coded levels of variables, but the hydrogen pressure was kept constant at 23 bar. To predict an optimization in the yield of *n*-C_{17} and *n*-C_{18} alkanes (dependent variables) a Box–Behnken DOE was selected within the same software, which automatically uses only the 15 best experimental data points from a total of 24 and was employed to fit a polynomial model. This model has three independent variables, i.e., temperature and reaction time were used as principal variables, and the third variable was selected from the following three: wt % Ni (W), average size of Ni nanoparticles (S), or coefficient of variation (CV) of Ni-nanoparticles size (V). This design led to three polynomial models to estimate the yield of *n*-C_{17} and another three models to estimate the yield of *n*-C_{18}. Equation 1 shows the quadratic polynomial for the prediction of alkanes yield:

$$Y = \beta_0 + \beta_1 X + \beta_2 T + \beta_3\ t + \beta_{12}\ X^2 + \beta_{13} XT + \beta_{23} Xt + \beta_{11} T^2 + \beta_{22} Tt + \beta_{33}\ t^2, \quad (1)$$

where $\boldsymbol{Y}$ is the yield of alkanes predicted, $\boldsymbol{T}$ is the temperature (°C), $\boldsymbol{t}$ is the reaction time (h), and $\boldsymbol{X}$ can take the value of any of the variables obtained in the analysis of the TEM micrographs as presented later. $\boldsymbol{X}$ can be $\boldsymbol{W}$, $\boldsymbol{S}$, or $\boldsymbol{V}$; $\boldsymbol{\beta_0}$ is the interception coefficient; $\boldsymbol{\beta_j}$s are linear terms; $\boldsymbol{\beta_{ij}}$s are interaction terms; and $\boldsymbol{\beta_{jj}}$s are square terms.

The software Statgraphics (Centurion XV, 2006, Stat Point Inc., (Warrenton, VA, USA) was used to obtain regression models from the response surface data. The statistical analysis was performed using analysis of variance (Anova). This analysis includes the Fisher ratio ($\boldsymbol{F}$) and the coefficient of determination ($\mathbf{R^2}$), which measures the fit of the polynomial model.

Table 7. Value range and coded levels of the independent variables.

Independent Variable	Symbol	Coded Levels		
		−1	**0**	**+1**
Temperature (°C)	T	320.00	330.00	340.00
Reaction time (h)	t	4.00	4.50	5.00
Ni loading, wt %	W	3.00	5.00	7.00
Average size of Ni NPs (nm)	S	3.03	4.41	5.58
CV of size distribution of Ni NPs (%)	V	32.40	32.51	34.29

4. Conclusions

Oleic acid is a relevant source for biodiesel production due to its presence in vegetable oils. A set of experiments with this organic acid and Ni/γ-Al_2O_3 as an appropriate catalyst were combined to study its HDO at different temperatures and reaction times. An increase in the amount of Ni deposited slightly decreases the amount of pores in the structure of the catalyst. The theoretical weight percentages of Ni NPs on alumina were in good accordance with the increasing amount of Ni on γ-Al_2O_3 detected by EDS analysis. Increasing Ni NPs on γ-Al_2O_3 leads to changes in the catalyst properties, raising intrinsic activity. Statistically, Ni nanoparticle parameters had a high interaction with the rest of the parameters regarding the n-C_{17} yield given by the ***p***-value. An optimal analysis for the maximum yields of n-C_{17} led us to identify 332 °C, reaction time of 4.78 h, combined with physical parameters of nanoparticles of 4.86 nm, and a distribution coefficient of 33.48%, very close to those provided by the NAL5 catalyst, as the optimal conditions for producing biofuel. Hence, considering the effects of Ni nanoparticles on the alkanes yield is important to achieve an affordable operation cost for this catalytic environmental process.

Acknowledgments: The authors would like to thank Regina Medina Rosales for reviewing writing of earlier versions of this paper. This research and paper publication was partially financed by Departamento de Posgrado e Investigación (Research and Postgraduate Department) of Universidad Politécnica de Aguascalientes (México) and Fomix (CONACYT-Mexico).

Author Contributions: M.S.-C. and J.M.V. conceived and designed the experiments; M.S.-C. performed the experiments; M.S.-C., J.M.V., S.-K.K. and R.R.M.R. analyzed the data; L.A.S.-O. contributed reagents/materials/analysis tools; M.S.-C., JMV, S.-K.K and R.R.M.R. wrote the paper.

Conflicts of Interest: The authors declare no conflicts of interest.

References

1. Puértolas, B.; Keller, T.C.; Mitchell, S.; Pérez-Ramírez, J. Deoxygenation of bio-oil over solid base catalysts: From model to realistic feeds. *Appl. Catal. B Environ.* **2016**, *184*, 77–86. [CrossRef]
2. Vasiliadou, E.S.; Lemonidou, A.A. Catalytic glycerol hydrodeoxygenation under inert atmosphere: Ethanol as a hydrogen donor. *Catalysts* **2014**, *4*, 397–413. [CrossRef]
3. Hu, J.; Yu, F.; Lu, Y. Application of Fischer–Tropsch Synthesis in biomass to liquid conversion. *Catalysts* **2012**, *2*, 303–326. [CrossRef]
4. Knothe, G.; Van Gerpen, J.H.; Krahl, J.J. *The Biodiesel Handbook*, 2nd ed.; AOCS PRESS: Champaign, IL, USA, 2010; pp. 1–24.
5. Yang, Y.; Ochoa-Hernández, C.; Pizarro, P.; de la Peña O'Shea, V.A.; Coronado, J.M.; Serrano, D.P. Influence of the Ni/P ratio and metal loading on the performance of Ni_xP_y/SBA-15 catalysts for the hydrodeoxygenation of methyl oleate. *Fuel* **2015**, *144*, 60–70. [CrossRef]
6. Kubička, D.; Horáček, J.; Setnička, M.; Bulánek, R.; Zukal, A.; Kubičková, I. Effect of support-active phase interactions on the catalyst activity and selectivity in deoxygenation of triglycerides. *Appl. Catal. B Environ.* **2014**, *145*, 101–107. [CrossRef]
7. Bezergianni, S.; Kalogianni, A.; Dimitriadis, A. Catalyst evaluation for waste cooking oil hydroprocessing. *Fuel* **2012**, *93*, 638–641. [CrossRef]
8. Ayodele, O.B.; Togunwa, O.S.; Abbas, H.F.; Daud, W.M.A.W. Preparation and characterization of alumina supported nickel-oxalate catalyst for the hydrodeoxygenation of oleic acid into normal and iso-octadecane biofuel. *Energy Convers. Manag.* **2014**, *88*, 1104–1110. [CrossRef]
9. Monnier, J.; Sulimma, H.; Dalai, A.; Caravaggio, G. Hydrodeoxygenation of oleic acid and canola oil over alumina-supported metal nitrides. *Appl. Catal. A Gen.* **2010**, *382*, 176–180. [CrossRef]
10. Hellinger, M.; Carvalho, H.W.P.; Baier, S.; Wang, D.; Kleist, W.; Grunwaldt, J.-D. Catalytic hydrodeoxygenation of guaiacol over platinum supported on metal oxides and zeolites. *Appl. Catal. A Gen.* **2015**, *490*, 181–192. [CrossRef]
11. Madsen, A.T.; Ahmed, E.H.; Christensen, C.H.; Fehrmann, R.; Riisager, A. Hydrodeoxygenation of waste fat for diesel production: Study on model feed with Pt/alumina catalyst. *Fuel* **2011**, *90*, 3433–3438. [CrossRef]

12. Yang, L.; Tate, K.L.; Jasinski, J.B.; Carreon, M.A. Decarboxylation of oleic acid to heptadecane over Pt supported on zeolite 5A Beads. *ACS Catal.* **2015**, *5*, 6497–6502. [CrossRef]
13. Ahmadi, M.; Nambo, A.; Jasinski, J.B.; Ratnasamyb, P.; Carreon, M.A. Decarboxylation of oleic acid over Pt catalysts supported on small-pore zeolites and hydrotalcite. *Catal. Sci. Technol.* **2015**, *5*, 380–388. [CrossRef]
14. Popov, S.; Kumar, S. Rapid hydrothermal deoxygenation of oleic acid over activated carbon in a continuous flow process. *Energy Fuels* **2015**, *29*, 3377–3384. [CrossRef]
15. Srifa, A.; Faungnawakij, K.; Itthibenchapong, V.; Assabumrungrat, S. Roles of monometallic catalysts in hydrodeoxygenation of palm oil to green diesel. *Chem. Eng. J.* **2015**, *278*, 249–258. [CrossRef]
16. Sitthisa, S.; Resasco, D.E. Hydrodeoxygenation of Furfural over Supported Metal Catalysts: A Comparative Study of Cu, Pd and Ni. *Catal. Lett.* **2011**, *141*, 784–791. [CrossRef]
17. Kong, X.; Zhu, Y.; Zheng, H.; Li, X.; Zhu, Y.; Li, Y. Ni Nanoparticles Inlaid Nickel Phyllosilicate as a Metal-Acid Bifunctional Catalyst for Low-Temperature Hydrogenolysis Reactions. *ACS Catal.* **2015**, *5*, 5914–5920. [CrossRef]
18. Olbrich, W.; Boscagli, C.; Raffelt, K.; Zang, H.; Dahmen, N.; Sauer, J. Catalytic hydrodeoxygenation of pyrolysis oil over nickel-based catalysts under H_2/CO_2 atmosphere. *Sustain. Chem. Process.* **2016**, *4*, 9. [CrossRef]
19. Onyestyák, G.; Harnos, S.; Szegedi, Á.; Kalló, D. Sunflower oil to green diesel over Raney-type Ni-catalyst. *Fuel* **2012**, *102*, 282–288. [CrossRef]
20. Tarditi, A.M.; Barroso, N.; Galetti, A.E.; Arrúa, L.A.; Cornaglia, L.; Abello, M.C. XPS study of the surface properties and Ni particle size determination of Ni-supported catalysts. *Surf. Interface Anal.* **2014**, *46*, 521–529. [CrossRef]
21. Matam, S.K.; Kondratenko, E.V.; Aguirre, M.H.; Hug, P.; Rentsch, D.; Winkler, A.; Weidenkaff, A.; Ferri, D. The impact of aging environment on the evolution of Al_2O_3 supported Pt nanoparticles and their NO oxidation activity. *Appl. Catal. B Environ.* **2013**, *129*, 214–224. [CrossRef]
22. Barzegar-Bafrooei, H.; Ebadzadeh, T. Synthesis of nanocomposite powders of γ-alumina-carbon nanotube by sol-gel method. *Adv. Powder Technol.* **2011**, *22*, 366–369. [CrossRef]
23. Li, G.; Hu, L.; Hill, J.M. Comparison of reducibility and stability of alumina-supported Ni catalysts prepared by impregnation and co-precipitation. *Appl. Catal. A Gen.* **2006**, *301*, 16–24. [CrossRef]
24. Wu, G.; Zhang, C.; Li, S.; Han, Z.; Wang, T.; Ma, X. Hydrogen production via glycerol steam reforming over Ni/Al_2O_3: Influence of nickel precursors. *ACS Sustain. Chem. Eng.* **2013**, *1*, 1052–1062. [CrossRef]
25. Moulder, J.F.; Stickle, W.F.; Sobol, P.E.; Bomben, K.D. *Handbook of X-ray Photoelectron Spectroscopy*, 2nd ed.; Eden Prairie: Hennepin County, MN, USA, 1995; pp. 89–117.
26. Obradović, A.; Likozar, B.; Levec, J. Catalytic surface development of novel nickel plate catalyst with combined thermally annealed platinum and alumina coatings for steam methane reforming. *Int. J. Hydrog. Energy* **2013**, *38*, 1419–1429. [CrossRef]
27. Chen, Y.S.; Kang, J.F.; Chen, B.; Gao, B.; Liu, L.F.; Liu, X.Y.; Wang, Y.Y.; Wu, L.; Yu, H.Y.; Wang, J.Y.; et al. Microscopic mechanism for unipolar resistive switching behaviour of nickel oxides. *J. Phys. D Appl. Phys.* **2012**, *45*, 065303. [CrossRef]
28. Shin, D.H.; Lee, J.S.; Jun, J.; Jang, J. Fabrication of amorphous carbon-coated NiO nanofibers for electrochemical capacitor applications. *J. Mater. Chem. A* **2014**, *2*, 3364–3371. [CrossRef]
29. Grosvenor, A.P.; Biesinger, M.C.; Smart, R.S.C.; Mcintyre, N.S. New interpretations of XPS spectra of nickel metal and oxides. *Surf. Sci.* **2006**, *600*, 1771–1779. [CrossRef]
30. Venezia, A.M.; Bertoncello, R.; Deganello, G. X-Ray Photoelectron Spectroscopy Investigation of Pumice-supported Nickel Catalysts. *Surf. Interface Anal.* **1995**, *23*, 239–247. [CrossRef]
31. Kang, W.; Tang, Y.; Li, W.; Yang, X.; Xue, H.; Yang, Q.; Lee, C. High interfacial storage capability of porous $NiMn_2O_4$/C hierarchical tremella-like nanostructures as lithium ion battery anode. *R. Soc. Chem.* **2014**, *1*, 24. [CrossRef] [PubMed]
32. Digne, M.; Sautet, P.; Raybaud, P.; Euzen, P.; Toulhoat, H. Use of DFT to achieve a rational understanding of acid-basic properties of γ-alumina surfaces. *J. Catal.* **2004**, *226*, 54–68. [CrossRef]
33. Šimáček, P.; Kubička, D.; Šebor, G.; Pospíšil, M. Hydroprocessed rapeseed oil as a source of hydrocarbon-based biodiesel. *Fuel* **2009**, *88*, 456–460. [CrossRef]

34. Kaewmeesri, R.; Srifa, A.; Itthibenchapong, V.; Faungnawakij, K. Deoxygenation of waste chicken fats to green diesel over Ni/Al_2O_3: Effect of water and free fatty acid content. *Energy Fuels* **2015**, *29*, 833–840. [CrossRef]
35. Kubička, D.; Kaluža, L. Deoxygenation of vegetable oils over sulfided Ni, Mo and NiMo catalysts. *Appl. Catal. A Gen.* **2010**, *372*, 199–208. [CrossRef]
36. Strobel, R.; Stark, W.J.; Mädler, L.; Pratsinis, S.E.; Baiker, A. Flame-made platinum/alumina: Structural properties and catalytic behaviour in enantioselective hydrogenation. *J. Catal.* **2003**, *213*, 296–304. [CrossRef]
37. Sotelo-Boyás, R.; Liu, Y.; Minowa, T. Renewable diesel production from the hydrotreating of rapeseed oil with Pt/zeolite and NiMo/Al_2O_3 catalysts. *Ind. Eng. Chem. Res.* **2011**, *50*, 2791–2799. [CrossRef]